Nuclear Materials and Energy 29 (2021) 101071

Contents lists available at ScienceDirect

Nuclear Materials and Energy

journal homepage: www.elsevier.com/locate/nme

Influence of the structural state and crystallographic texture of Zr-2.5% Nb alloy samples on the anisotropy of their thermal expansion

M.G. Isaenkova, A.V. Tenishev, O.A. Krymskaya, S.D. Stolbov *, V.V. Mikhal'chik, V. A. Fesenko, K.E. Klyukova

National Research Nuclear University "MEPhI"

ARTICLE INFO

Keywords:
Anisotropy
Thermal expansion
Zr-alloys
Crystallographic texture
Phase transformation

ABSTRACT

Zirconium remains the main structural material for thermal reactors due to the small capture cross section of thermal neutrons. In the period of stricter safety requirements for reactors with a simultaneous increase in operating parameters, predicting the behavior of the material in emergency situations has gained greater urgency. In this work, we measured the temperature dependence of the thermal expansion of samples cut from thick-walled tubes made of Zr-2.5% Nb alloy that were deformed and annealed in different modes. The analysis of the physical processes responsible for the shaping of the material is carried out. It was found that the anisotropic change in the linear dimensions of cubic samples both during heating and cooling is due to a change in the zirconium content in the β-phase, phase transformations $\alpha + \beta\text{-Zr} \rightarrow \alpha + \beta\text{-Nb} \rightarrow \beta \rightarrow \alpha + \beta\text{-Zr}$, as well as the preferred orientation of the grains of the α-phase, characterized by high anisotropy of linear expansion. It is shown that the expansion of the investigated samples upon heating in the α -phase is determined exclusively by the integral texture parameters of Kearns, and the coefficients of thermal linear expansion (TLEC) in different directions vary over a wide range from $3{\cdot}10^{-6}$ to $12{\cdot}10^{-6}$ K^{-1}. During cooling at the stage of the reverse phase transformation of the β-phase into α, an increase in the size of the cubic samples in the tangential direction up to 2.3 % and a decrease in the radial direction to 1.3 % are noted, which is associated with the orientation of the α-phase grains formed during cooling in the β -matrix and anisotropy of the TLEC of the α -grains. It is shown that the orientation of the α-phase grains in the reverse $\beta \rightarrow \alpha$ transformation is determined not only by the orientation of the basal axes in the initial material, but also by the spatial distribution of the prismatic axes relative to the external directions in the tube. Significant size fluctuations in different directions of the samples obtained using the technology of manufacturing channel tubes for CANDU reactors should lead to the development of significant macrostresses both during heating and cooling of the tube. The structural state of the samples deformed or annealed at 400–530 °C does not significantly affect the temperature dependence of the TLEC, but is manifested only in some of its features. In this case, completely recrystallized samples, i.e., with a recrystallization texture, in which the $< 11\bar{2}0 >$ directions are oriented along the tube axis, are characterized by a significantly lower variation in dimensions in different directions in the temperature range 20–1200 °C.

Introduction

Low-alloyed zirconium-based alloys are the main structural materials of the core of thermal reactors [1–2] due to the optimal set of operational characteristics. However, the crystal structure of the low-temperature modification of hexagonal zirconium causes significant anisotropy of thermal expansion of products made of alloys based on them [2–3]. As a result of the anisotropic expansion of grains of different orientations, stresses arise at the boundaries between them, which can relax at different temperatures using a variety of processes that are realized in polycrystalline materials. In addition, an increase in temperature affects the change in the dimensions of the operated products, which ensures the appearance of macrostresses in the construction as a whole, causing thermal creep and even the occurrence of cracks [4–6]. The behavior of the material with increasing temperature is an integral part of the processes occurring in the product under the additional effect

* Corresponding author.
E-mail addresses: isamarg@mail.ru (M.G. Isaenkova), avt@onil709.ru (A.V. Tenishev), olgakrym@inbox.ru (O.A. Krymskaya), stolbser@rambler.ru (S.D. Stolbov), vladimir_mephi@mail.ru (V.V. Mikhal'chik), fesenko.vlad@mail.ru (V.A. Fesenko), tinakyukova@gmail.com (K.E. Klyukova).

https://doi.org/10.1016/j.nme.2021.101071
Received 12 May 2021; Received in revised form 2 September 2021; Accepted 3 September 2021
Available online 11 September 2021

of neutron irradiation [7–9]. Predicting the behavior of such materials during thermal expansion is an urgent problem, as evidenced by the works of various authors [10–12], and should be based on systematic dilatometric and structural studies. In the context of an intensive search for coating materials for creating tolerant cladding tubes [13–23], the issues of thermal expansion of cladding tubes designed for emergency situations are of primary importance.

Among the publications, it is worth noting a review of computational codes MATPRO for determining the properties of oxide fuel and cladding tubes with subsequent variations and generalizations [10,11], in which data from different authors are combined and analyzed and the calculated dependence of the elastic and thermophysical properties of zircaloy of different compositions are presented. The calculation of the coefficients of thermal linear expansion (TLEC) for the axial and tangential directions of cladding tubes made of zircaloy is carried out in the MATPRO code [12,13] based on the data for single crystals of zircaloy obtained in [12] and the volume fractions of crystallites of the corresponding orientations. The FRAPCON-4.0 code [11] differs from MATPRO in that the calculation within the range up to 1000 °C is based on the data of the authors [24–26] and does not require texture data. Above 1000 °C, TLEC are considered as a constant value equal to 9.7×10^{-6} K^{-1}. In the area of phase transformation into zircaloy (800–1000 °C), the coefficients are determined by linear interpolation, which is due to the stability of the α-structure up to a temperature of 800–980 °C. In Russian alloys Zr-1% or 2.5% Nb phase transformation begins already at a temperature of 600–630 °C, which leads to significant volumetric changes and deformation of products [27–29]. According to the results of these studies, when the temperature of the two-phase region is reached, the change in the composition of the β-phase and the actual α → β phase transformation itself provide a significant anisotropic decrease in the sample size, which explains the development of significant stresses in different directions of the objects under study. It was found in [27] that the niobium content of 1 % and 2.5 % practically does not affect the expansion anisotropy of the material, since for the equilibrium state of these alloys, the amount of the β-phase changes insignificantly (from about 0.4 to 2.1 %) and the composition of the α -phase determining the anisotropy of the TLEC is the same.

The temperature dependence of the TLEC makes it possible to understand the physical processes occurring in alloys during heating and cooling at different temperatures. Knowledge of the regularities of changes in the external dimensions of the product during heating and cooling will purposefully create the structural-phase state and crystallographic texture of the material, providing minimal dimensional changes.

Along with the data on thermal expansion, the crystallographic texture turns out to be a sensitive indicator to the processes occurring during phase transformations and recrystallization [30–34]. It is for this reason that the behavior of the product under thermal expansion is predicted from the data on the orientation of the basal axes [29,35–36]. It should be noted that the orientation of the prismatic axes should also affect the development of processes that determine the final dimensions of the products. The prismatic normal orientation determines the orientation of the β-phase at the heating stage and, consequently, the subsequent features of the nucleation of grains of the anisotropic α-phase upon cooling from the temperature of the single-phase region of the existent β-phase [37–39].

The phase transformation in zirconium occurs in accordance with the orientational Burgers relation [3]. The regularities of phase transformations depend on many factors, for example, on the preliminary treatment (the deformation degree) of the material [39], the distribution of work hardening [33,40], and the rate of heating and cooling of the material [38,41–42]. It was shown in [38] that preliminary cold deformation slows down the process of phase transformation (PT). The dependence of the α → β phase transformation on the work hardening distribution in grains of different orientations is illustrated in [33,40]. It was shown in [38,42] that during rapid cooling (quenching in water), α-plates nucleate inside the β-phase grains, and during slow cooling (cooling with a furnace or in air), the centers of α-phase nucleation are predominantly interphase α/β-boundaries.

This work is devoted to the study of the influence of the structural-phase state and the preferred orientation of grains of the Zr-2.5% Nb alloy on the process of thermal expansion of samples cut from the wall of tube billets.

Materials and methods

Table 1 presents elemental content of studied alloys.

Dilatometric studies were carried out on cubic specimens cut from zirconium tubes made of Zr-2.5% Nb alloy, the wall thickness of which varied from 4.2 to 4.8 mm. Table 2 presents a description of the studied samples with an indication of their phase composition and integral texture parameters. The relative fraction of β-Zr in this alloys is within 7 ÷ 9% with average size of grains 0.5 ÷ 1.5 μm.

A schematic of cutting samples for the dilatometric studies is shown in Fig. 1. The samples were cut out by the electric spark method; kerosene was used as a cooling medium. For each state, three samples were prepared, the dimensions of which were 4 × 4 × 4 mm. The edges of the cubic specimens prepared by grinding followed by etching in the mixture of HF, HNO_3 and water coincided with the main outer directions of the tubes: radial *R*, tangential *T*, and axial *L*. The obtained specimens were used to measure their expansion in three mutually perpendicular directions: *R*, *T*, and *L*, in the temperature range 20–1200 °C.

The study of thermal expansion was carried out on a Netzsch 402C dilatometer in a high-purity helium flow (99.9999 %) with its additional purification with a Monotorr getter catalytic filter. In addition, an additional oxygen getter OTS manufactured by Netzsch was located next to the sample. The dilatometric experiment technique is described in detail in the works [28–29].

X-ray studies of the structure and crystallographic texture of the cubic samples before and after dilatometry were carried out on diffractometers DRON-3 and D8 Discover using Cr K_α and Cu K_α radiation, respectively. The analysis of the crystallographic texture of polycrystalline materials was carried out by X-ray diffractometric recording of incomplete direct pole figures (DPF) {*HKL*} by the method of tilting the sample for the corresponding reflections (*hkl*). The method for studying the crystallographic texture of articles made of zirconium-based alloys is described in detail in [34,43]. Incomplete DPFs (0001) and $\{11\bar{2}0\}$ were recorded up to tilt angles of 70°, respectively. From the incomplete DPFs, taken from three mutually perpendicular sides of the cubic sample, the complete DPFs were reconstructed by the cross-linking method for its cross section perpendicular to the *R*-direction. The DPF (0001) was used to calculate the integral texture parameters of Kearns [27,44], which are the sum of the effective fractions of the basal axes [0001] oriented along the chosen direction in the polycrystal. These parameters are used to assess the properties of a textured material with known properties along crystallographic axes *a* and *c* for a hexagonal single crystal [33,44].

Results and discussion

Structure and crystallographic texture of the original samples

The material of the cold-rolled tube (sample No. 1) contains two metastable phases α- and β-Zr, as evidenced by the diffraction patterns shown in Fig. 2-a. During deformation in the distorted crystal structure

Table 1
Chemical composition of researched samples

Nb	Fe	O	Zr
2.5 ÷ 2.8	<0.065	0.10 ÷ 0.14	balance

Table 2
Description of the studied samples from the Zr-2.5% Nb alloy

Sample number	The final stage of tube processing	Phase composition	Integral texture parameters		
			f_R	f_T	f_L
1	cold rolling	α-Zr и β-Zr	0.38	0.55	0.07
2	annealing at 400 °C – 24 h	α-Zr, ω-Zr и β-Zr	0.36	0.59	0.06
3	annealing at 530 °C – 3 h	α-Zr и β-Zr	0.35	0.55	0.10
4	annealing at 580 °C – 3 h	α-Zr и β-Nb	0.56	0.40	0.04

of the α- and β-phases, an additional amount of alloying elements, as compared to the equilibrium phase diagram, dissolves [33,45–47]. Therefore, the lines of both phases are characterized by significant broadening. β-phase is a solid solution of niobium in β-Zr. Broadening of diffraction lines can indicate both a high distortion of the structure of the deformed material and a variation in the niobium content in the solid solution of bcc zirconium (the Nb content in β-Zr is about 16 – 20 % according to Vegard's law). The lines of the α-phase are slightly shifted towards small Bragg angles (Fig. 2-a), which indicates an increase in the interplanar distances in the deformed material due to the high concentration of dislocations and the presence of macrostresses in the deformed tube. From the fragments of the diffraction patterns in Fig. 2, it follows that sample No. 2 consists of α-, β-Zr, and ω-phases. It is shown in [3,33,48] that annealing of the β-phase with a niobium content of more than 17 % in the temperature range of 350–450 °C for 5–10 h leads to the formation of the ω-phase in the β-phase. Electron microscopic images of the ω-phase inside the β-grains in the Zr-2.5% Nb alloy are presented in [49–50]. Sample No. 3 consists of α- and β-Zr phases, which indicates the incompleteness of the process of redistribution of niobium between phases to concentrations corresponding to the equilibrium phase diagram. Sample No. 4 consists of α-Zr and β-Nb phases corresponding to the equilibrium phase diagram.

Fig. 3 shows DPFs (0001) and $\{11\bar{2}0\}$ for deformed (sample No. 1) and annealed at temperatures of 530 (No. 3) and 580° C (No. 4) tubes, and Table 1 shows the integral texture parameters for all investigated samples. According to the obtained results, samples Nos. 1, 2, and 3 are characterized by practically the same preferred orientation, which can be described by the texture component $\{11\bar{2}0\} < 10\bar{1}0 >$. The stability of the deformation texture in the samples annealed at temperatures of 400 and 530 °C indicates the occurrence of recovery processes (annealing of point defects and polygonization), in which the orientation of the basal and prismatic axes does not change. Annealing of deformed products at a temperature of 580 °C leads to a redistribution of basal and prismatic axes (Fig. 3-c), which is caused by the growth of grains misoriented relative to the deformed matrix by an angle of 30° around the basal axes, as shown in [33,50–52]. In the latter case, a recrystallization texture is formed; therefore, these samples No. 4 will be called recrystallized, in contrast to samples No. 2 and No. 3.

Anisotropy of thermal expansion of pressure tubes made of Zr-2.5% Nb alloy

Fig. 4 shows the temperature dependence of the change in the dimensions of the annealed and deformed samples, measured during their heating (solid lines) and cooling (dashed lines) in the temperature range 50–1200 °C. The results of testing cubic samples in different directions *R*, *T*, and *L* are shown in Fig. 4 curves of different shades: black - *R*, gray - *T*, and light gray - *L*.

The linear dimensions of the samples were also measured before and after the temperature tests. At the same time, different changes in dimensions were recorded in different directions, which for the annealed samples are given in Table 3. The measurements of the dimensions of the samples are in good agreement with the results presented in Fig. 4.

On the cubic samples, it is convenient to study the anisotropy of expansion or contraction as a result of the heating–cooling cycle in the temperature range of 50–1200 °C, since in this case, the other directions

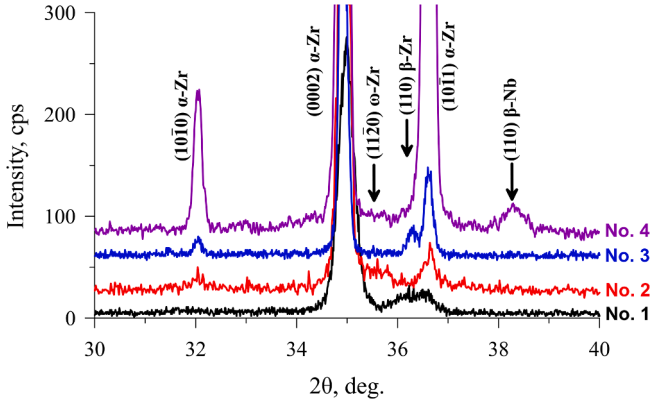

Fig. 2. Diffraction patterns of the studied samples in the deformed (No. 1) and annealed at 400 °C – 24 h (No. 2), 530 °C – 3 h (No. 3) and 580 °C – 3 h (No. 4) states. In the figure, the arrows show the positions of the lines of different phases.

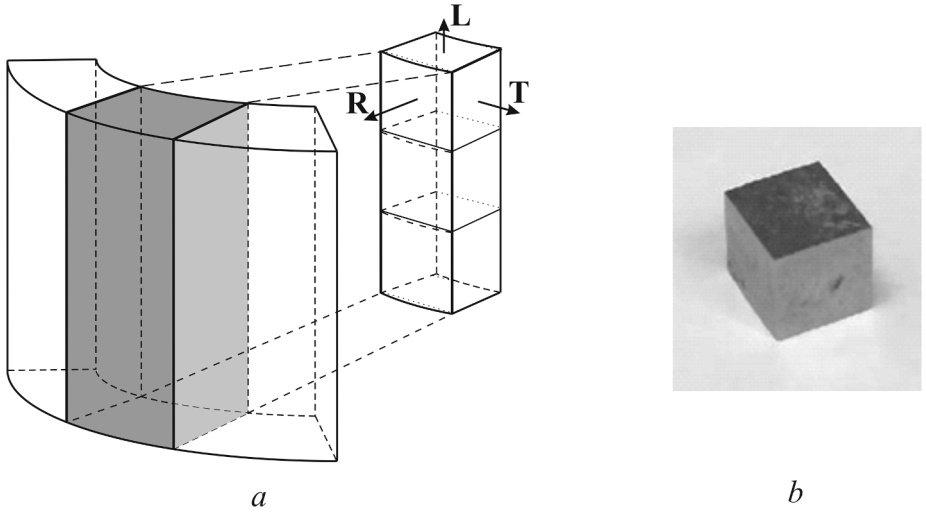

Fig. 1. Scheme of cutting samples from the pressure tube (a) and the appearance of the prepared sample (b).

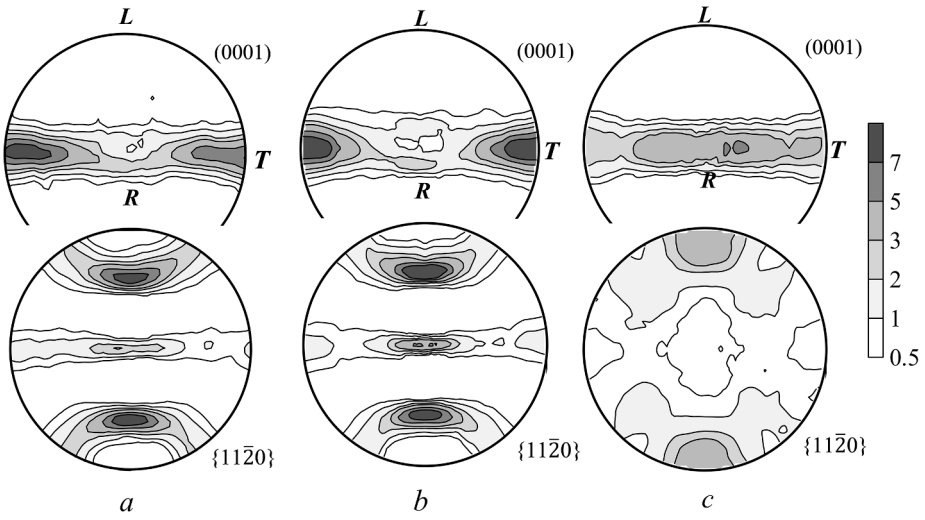

Fig. 3. Texture of cold-rolled samples (No. 1, a) and samples annealed at 530 °C (No. 3, b) and at 580 °C (No. 4, c). DPFs (0001) and {11$\bar{2}$0}

do not affect the result of the change in dimensions, as is observed in the case of testing tubular samples. According to the presented data for samples No. 1–3, an increase in the sample size by 1.9–2.3 % occurs in the direction of orientation of the basal axes. In this case, along the radial direction, a decrease in the sample size by 0.8–2.0 % is recorded, which is comparable to the changes in size along the tangential direction, although it is half as much. Note that the axes < 11$\bar{2}$0 > are oriented along the radial direction, as well as some fraction of the basal axes. An increase in sample dimension is recorded along the axial direction by only 0.1–0.3 %.

It should be noted that dilatometric measurements are carried out using a pusher, which at room temperature creates a force on the sample of 40 cN, i.e., stresses are about $2{\cdot}10^3$ Pa. However, even such low stresses at high temperatures can cause plastic deformation of samples, especially at temperatures corresponding to dynamic processes of recrystallization or PT. So, when testing recrystallized cladding tubes with thin walls (<0.7 mm) along the *L*-direction, the beginning of a decrease in size is recorded already at 527° C [28–29]. In the latter case, the stresses acting in the axial direction are about 10^4 Pa. The possibility of the development of circumferential (tangential) stresses in tubular specimens should also be taken into account. The effect of the pusher on the value of the final dimensions of the cubes is expressed in an additional reduction in dimensions in the direction of the action of the compressive forces during the test. Thus, when the specimen is compressed in the *R*-direction, its deformation is −1.0 %, while with the deformation in the T-direction, it is −0.8 %. However, it should be noted that the compression of the specimen in the *R*-direction decreases to −1.3 % when subjected to compressive forces along the *L*-direction. This contradiction, apparently, is associated with the anisotropy of the change in size due to the crystallographic texture of the samples under study.

The temperature dependence of the change in the linear dimensions in the radial direction turned out to be the most sensitive to the beginning of PTs, which begin in the bulk of the material at lower temperatures. This behavior is due to the following processes in the sample. The axes are oriented near the radial direction (see Fig. 3) [0001] and < 11$\bar{2}$0>; that is, grains with different orientations are present. The expansion of grains with different orientations along the *a* and *c* directions of the crystal structure occurs in different ways [28,3]. Therefore, stresses arise, the relaxation of which near the temperature of the onset of recrystallization and the motion of high-angle boundaries can occur both due to the acceleration of diffusion processes and due to the activation of plastic deformation under conditions of nonequilibrium structure. Then, on the thermal expansion curve, the onset of the transition from expansion to compression of both annealed and deformed samples shifts to a temperature of 550 °C. Naturally, the PT process is affected by the same expansion anisotropy of grains of different orientations and an increase in stresses between these grains.

It is more convenient to consider the specific features of the change in the slope of the dilatometric curves in the region of the PT flow using the temperature dependence of the TLEC.

Coefficients of thermal linear expansion (TLEC)

The temperature dependence of the TLEC for the deformed (sample No. 1, a) and annealed samples Nos. 2 and 4 (b) is shown in Fig. 5. The general character of the curves over the entire investigated temperature range is approximately the same. Distinctive features of the curves under consideration are the presence of clearly defined boundaries of the change of processes affecting the dimensional changes in the annealed samples and their slight blurring on the curves for deformed samples. The temperature dependence of the TLEC are presented on two scales of the temperature scale: in Fig. 5A, the temperature range of 50–1200 °C is considered, and in Fig. 5B, the features of low-temperature (100–600 °C) expansion of the studied samples are demonstrated.

Comparison of dilatometric curves of deformed and annealed samples in the low-temperature region (up to 580 °C)

In the alloy annealed at a temperature of 580 °C (sample No. 4), a linear dependence of TLEC on temperature is observed in the region of existence of equilibrium α-Zr and β-Nb. In this case, the TLEC values for different directions are determined by the integral texture parameters, as was shown in [26,27]. According to the thermal expansion data for sample No. 4, i.e., temperature dependence of the TLEC on the integral texture parameter along the chosen direction in the sample $\alpha_N = f_N{\cdot}\alpha_c + (1 - f_N){\cdot}\alpha_a$, and under the assumption that the crystallographic texture is constant during the dilatometric tests, the temperature dependence of TLECs α_a and α_c for the α-phase of the Zr-2.5% Nb alloy is calculated. The dependence of TLECs α_a and α_c for the α-phase of the Zr-2.5% Nb alloy and for pure polycrystalline zirconium [3] is compared in Fig. 6. The obtained values of TLEC α_a and α_c for the α-phase of the Zr-2.5% Nb alloy were used to estimate the TLEC of samples Nos. 1–3 in different directions in terms of texture parameters and are presented in Table 4 for the temperature range 100–400 °C.

From the presented data on the deviation of the calculated and measured TLECs, it follows that the structural state of the material has a significant effect on the thermal dependence of the TLEC. Let us consider

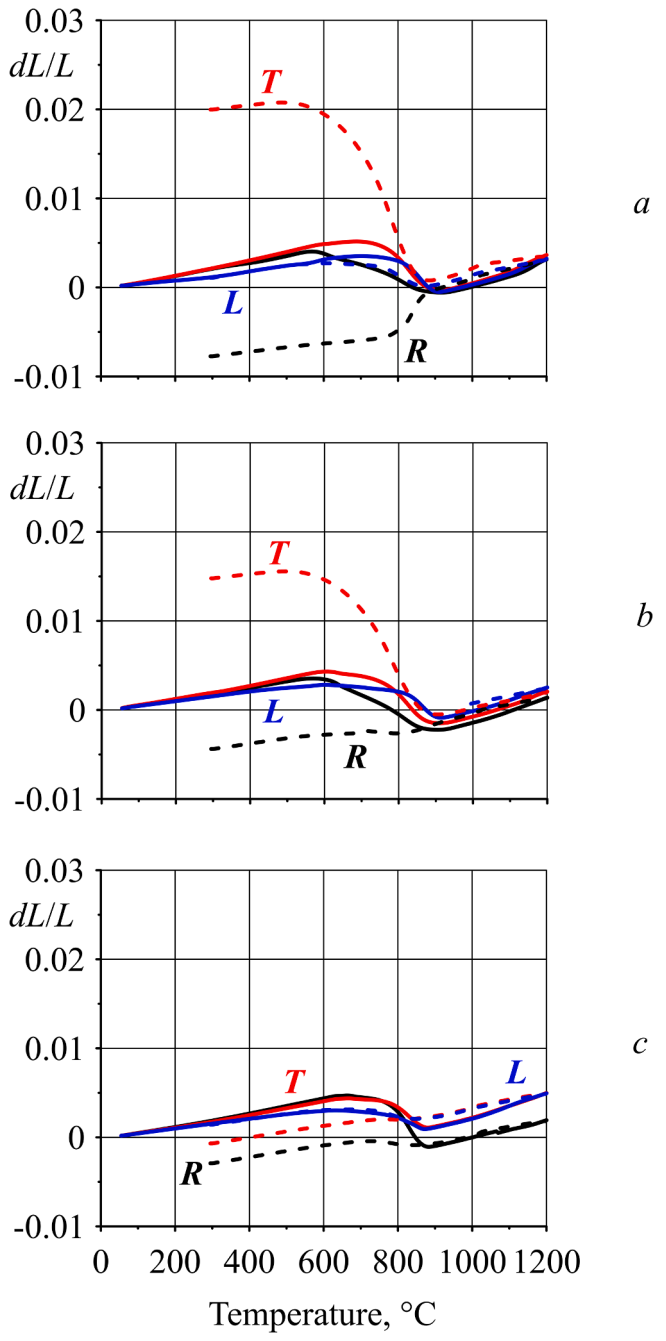

Fig. 4. Dilatometric curves of heating (solid lines) and cooling (dashed lines) deformed (a) and annealed (b, c) cubic specimens in three directions (samples No. 1, a; No. 3, b; and No. 4, c).

in more detail the obtained temperature dependence shown in Fig. 5.

The structures of the deformed (sample No. 1) and annealed at 400 °C (sample no. 2) differ fundamentally. In the deformed material, along with a large number of dislocations, there is a β-zirconium phase with an increased crystal lattice parameter relative to the lattice parameter of the β-niobium or ω-phase, the latter being formed as a result of annealing at a temperature of 400 °C. Since the annealed material is stable at least at temperatures below 400 °C, the dependence of the TLEC for different directions are practically linear. The TLEC value is determined by the integral texture parameters. The change in the TLEC for different directions can be associated with changes in the parameters of the crystal structure of the α-phase prevailing in the alloy, which, according to [28,29,3], increases in the presence of the [0001] axes in this direction and decreases or remains constant along the $< 11\bar{2}0 >$ axes.

Table 3
Change in the dimensions of cubic samples as a result of a cycle of thermal tests in the temperature interval 50–1200 °C

Sample number	Test direction	Resizing the sample, %			Annealing mode
		R	*T*	*L*	T °C - time in h
2	*R*	−1.0	2.3	0.30	400 °C – 24
	T	−0.8	2.1	0.08	
	L	−1.3	1.9	0.04	
3	*R*	−2.0	1.6	0.4	530 °C – 3
	T	−1.6	1.5	0.1	
	L	−0.5	1.1	−0.6	
4	*R*	−0.2	0.1	0.1	580 °C – 3
	T	−0.1	−0.1	0.2	
	L	−0.3	−0.1	0.1	

When the heating temperature exceeds 400 °C, the stability of the system is violated, which leads to a change in the slope of the temperature dependence of the TLEC in the corresponding direction. TLEC in the *L*-direction decreases, while in the *T*- and *R*- directions, on the contrary, it increases. The observed anisotropy of the expansion of the samples is due to the predominant orientation of the basal axes in the *R*-*T* plane, perpendicular to the axial direction *L*.

The temperature dependence of the TLEC for the annealed sample tested in the axial direction (light gray curve in Fig. 5-b) at a temperature of 510–520 °C shows a small maximum associated with the transition of the ω-phase to the β-Nb phase. A maximum shift to a temperature of 480 °C is also noted on the curve for the *R*-direction. Taking into account that the ω-phase is very finely dispersed, its transformation into the β -Nb phase remains practically unnoticed for the *T*-direction, which characterizes the expansion of the α-phase grains prevailing in the alloy along the basal axes.

The temperature dependence of the TLEC for the tangential direction is characterized by a continuous increase up to 540 °C. In this case, the temperature curves of the TLEC for the axial and radial directions of the deformed sample have a sinusoidal shape. Starting from 250 °C, an increase in the TLEC is observed in the axial direction, and a decrease in the TLEC in the radial direction. After 380–420 °C, the trend of changing TLEC for these directions is reversed, i.e., for the *L*-direction, a decrease in TLEC is observed, and for the *R*-direction, an increase.

In a deformed material (Fig. 5, B-a), with an increase in temperature, diffusion processes of redistribution of niobium in phases begin with the simultaneous movement of deformation defects. Since the deformed material contains non-equilibrium-zirconium (see Fig. 2), the concentration of niobium in the α-phase also does not correspond to the equilibrium one; more niobium is dissolved in it than in the annealed material. All phases present in the alloy expand according to their own laws. β-zirconium has a TLEC more than α-zirconium. In addition, grains of different orientations expand in different ways. In addition, it is necessary to take into account the movement of dislocations. It was shown in [28] that at temperatures above 300 °C, the mobility of dislocations, which were blocked by Cottrell atmospheres, is facilitated. In a deformed material, this process, apparently, begins already at a temperature of 250 °C and is expressed in a significant change in the TLEC in the *R*- and *L*- directions. Since most of the dislocations have a Burgers vector $< 11\bar{2}0 >$, their sliding causes a rearrangement of the structure along the indicated crystallographic directions perpendicular to the basal normal. Such an improvement in the structure due to the motion of dislocations does not affect the expansion of grains in the tangential direction, along which the basal axes are predominantly oriented, and significantly affects the change in grain sizes along the prismatic axes.

After the annealing of the defects, the TLECs approach the values characteristic of the annealed material. This is followed by the PT area, which is discussed below.

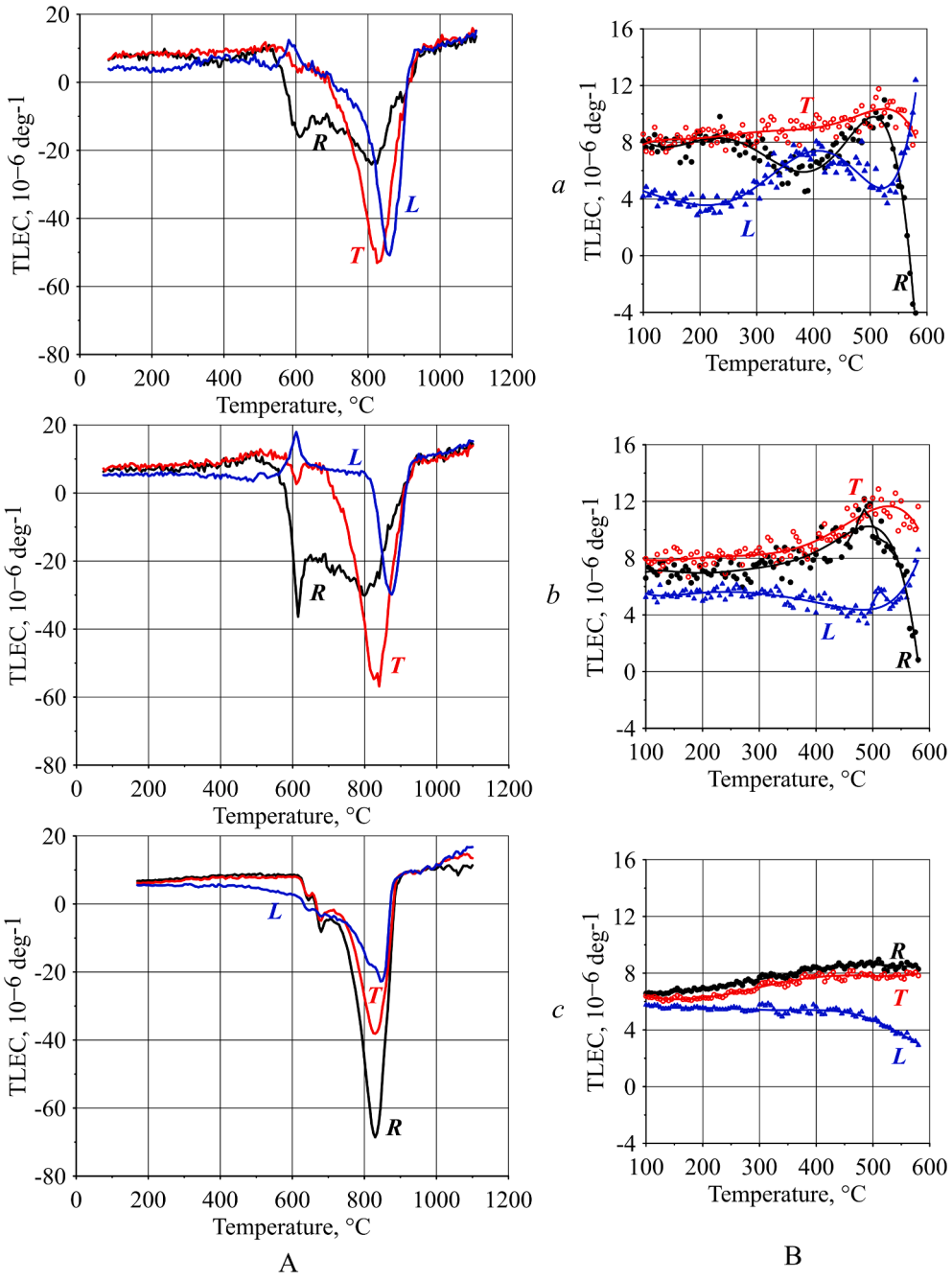

Fig. 5. Temperature dependence of TLEC obtained for cubic deformed (a) and annealed at temperatures of 400 (b) and 580 °C (c) in three main directions *R*, *T*, and *L*. A and B – different temperature ranges.

Analysis of the temperature dependence of the TLEC of deformed and annealed samples in the high-temperature region (above 580 °C)

At temperatures above 600 °C, in accordance with the phase diagram of the binary Zr-Nb alloy [3], the transition of β-Nb to β-Zr begins, at which the amount of the β-phase increases from 2.2 % to 10.6 % (the concentration points on the monotectoid line of the phase diagram correspond to 0.6, 18.5, and 88 at.% Nb). An increase in the amount of β-phase contributes to a decrease in TLEC, as was shown in [29]. This α → β phase transformation occurs with a decrease in the volume of the unit cell. Furthermore, the course of the PT will be associated with a sharp decrease in the TLEC. The PT process occurs most uniformly on samples No. 4 recrystallized at 580 °C. PT begins in accordance with the phase diagram of the Zr-Nb alloy at about 610–620 °C and ends at a temperature of 850–860 °C, at which the TLEC returns to the initial level of about $9{\cdot}10^{-6}K^{-1}$. The minimum TLEC values for different directions are characterized by different values, but the minimum TLEC is observed practically at the same temperature, at about 820 °C.

The temperature dependence of the TLEC of the remaining samples Nos. 1–3 have a more whimsical form, which is due to the nonequilibrium initial state of the material of these samples. The onset of the PT shifts to lower temperatures of 550–580 °C; the curves show two extrema, which differ significantly for different directions of testing. For example, in the *L*-direction, there is a sharp increase in TLEC. An increase in the TLEC for the *L*-direction can be associated with the peculiarities of the distribution of microstresses in the sample with a tangential texture (see DPF (0001) of the samples after the PT in Fig. 7),

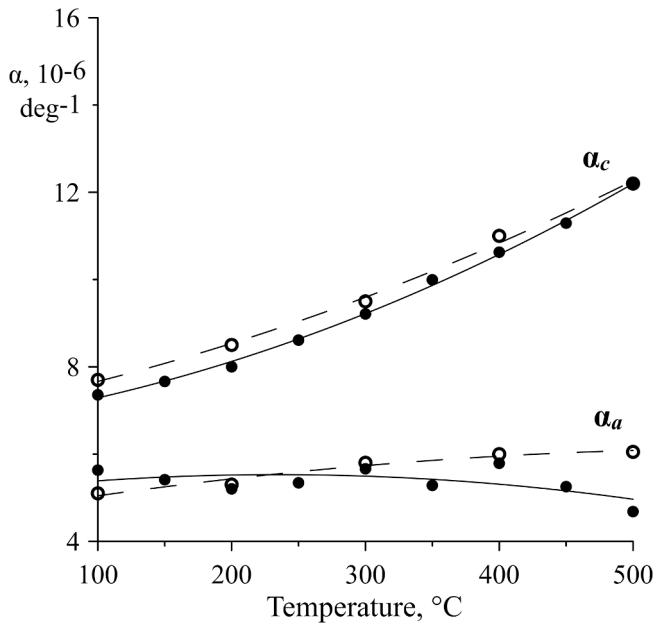

Fig. 6. Comparison of the temperature dependence of TLEC for the α-phase of the Zr-2.5% Nb alloy (solid lines) and pure zirconium (dashed lines).

at which compression occurs along the *R*- and *T*-directions, and the size slightly increases along the *L*-direction with a general decrease in volume associated with α → β PT. Another reason for the increase in the TLEC in the *L*-direction may be a change in the niobium concentration in the β-phase and an increase in the bcc lattice parameter, as a result of which the latter changes from 3.33 Å to 3.58 Å, i.e., more than 7 %. But, since the diffusion process does not occur simultaneously, this process of niobium redistribution is associated with a certain temperature range.

In the temperature range 590–620 °C, the main process is the phase transition of the α-phase in β associated with a decrease in the linear dimensions [29]; therefore, sharp minima are observed on the temperature dependence of the TLEC. The first minimum values are present on the curves for the *R*- and *T*-directions when testing annealed (400–530 °C) and deformed samples in the range 600–610 °C (Fig. 5 A). Furthermore, with an increase in the heating temperature of the samples, the process of joint expansion of both phases develops with a gradual increase in the amount of the β-Zr-phase from 10.6 to 100 % and a simultaneous change in its composition from 18.5 to 2.5 % Nb. The obtained temperature dependence of the TLEC for different directions of testing (Fig. 5A) indicates that the phase transition occurs in different times in grains of different orientations. PT in all samples tested in three directions occurs in the same temperature range from 580 to 920 °C. However, if the PT in the samples tested in the *R*-direction, after a minimum at a temperature of 610 °C, the TLEC remains negative, then in the samples tested in the *T*- and *L*-directions, the PTs proceed some differently. After the section with the minimum TLEC value (580–620 °C), the expansion process of the sample is restored with practically the same TLEC value (a plateau is observed on the corresponding curves). Such stability of the TLEC is retained for the longest time (up to 800 °C, Fig. 5A-b) during the expansion of the sample in the *L*-direction. The temperatures of the minimum values on the temperature dependence of TLEC (Fig. 5 a, b) are shifted relative to each other for the curves *R*, *T*, and *L* and are 800, 830, and 880 °C, respectively.

The shift of the minima on the temperature dependence is associated with the dynamics of the processes occurring in the material. At the initial stages of PT, i.e., after the temperature of the monotectoid line is exceeded and the concentration of zirconium in the bcc phase changes, the process of formation of the β-phase from energy representations should proceed uniformly in the volume of the sample. Since α → β PT occurs strictly in compliance with the orientation ratio, then the final texture should repeat the blurring of the original maximum. This process is observed for completely recrystallized sample No. 4, as evidenced by the appearance of texture maxima along the *R*-*T*-diameter of the stereographic projection (Fig. 7-b).

In the case of samples Nos. 1–3, the process proceeds somewhat differently, which is confirmed by the DPF (0001) and {11$\bar{2}$0} shown in Fig. 7. If phase transformations start from the boundaries, then, most likely, the nuclei of the phase should be grains of the β-phase present in the alloy, regardless of the stage at which it was formed, i.e., at rolling or as a result of transformation from the omega-phase. Since all phase transitions are related by crystallographic orientation relationships, the orientation in the newly formed phase is strictly maintained. The orientation of the bcc phase in the rolled samples is characterized by the texture component {001} ⟨110⟩ . This is confirmed by a large number of studies [38,40,49]. Since the texture of the original tube is formed as a result of its hot extrusion, i.e., in the β or (α + β)-region of the phase diagram, then all the formed phases in one way or another inherit exactly the texture of the high-temperature phase {001} ⟨110⟩ . Considering that most of the α-grains correspond to the orientation of the basal axes in the tangential direction, these grains prevail in the bulk of the material. The growth of such grains and the absorption of grains of a different orientation explain the deep minimum in the temperature dependence of the TLEC in the *T*-direction. The TLEC curve for the *L*-direction follows the curve for the tangential direction with some delay.

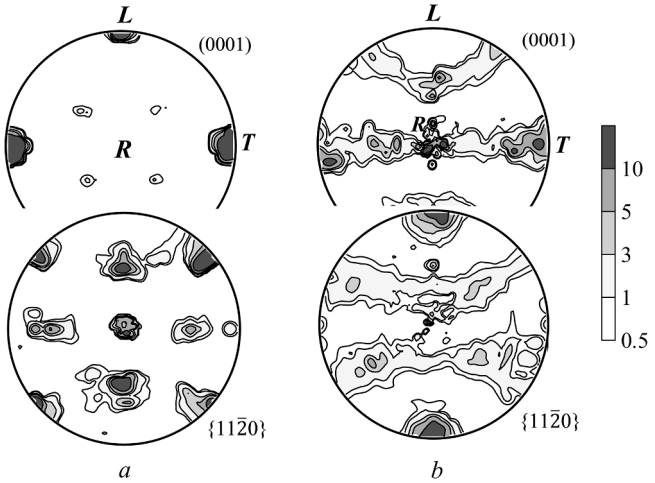

Fig. 7. DPFs (0001) and {11$\bar{2}$0} of deformed (No. 1, a) and annealed at 580 °C (No. 4, b) specimens after thermal tests in the *R*-direction.

Table 4
Limits of the TLEC change in the temperature range 100–400 °C

Sample number	TLEC, 10^{-6} K^{-1} (calculation)			TLEC, 10^{-6} K^{-1}(experiment)			Δ(TLEC)/TLEC, %		
	R	*T*	*L*	*R*	*T*	*L*	*R*	*T*	*L*
1	6.3÷7.7	6.4÷8.0	5.4÷6.1	6.6÷8.6	7.7÷9.3	3.1÷7.2	4÷22	10÷26	11÷42
2	6.2÷7.5	6.6÷8.6	5.4÷6.1	6.6÷8.3	7.8÷8.8	5.2÷5.9	5÷18	1÷23	3÷18
3	6.2÷7.5	6.6÷8.5	5.5÷6.3	5.6÷7.3	6.4÷8.5	5.3÷5.6	1÷10	1÷6	1÷14
4	6.6÷8.3	6.2÷7.8	5.1÷5.8	6.6÷8.3	6.2÷7.8	5.1÷5.8	–	–	–

A decrease in the TLEC value in the PT temperature range (580–920 °C) may be associated with the additional development of plastic deformation under conditions of structural instability of the material. In the case of the action of compressive stresses in the radial direction, the process of plastic deformation of the α-phase easily develops over all possible slip systems. In the case of the tangential direction, this process is somewhat more difficult to activate, but given that there are grains deviated from the tangential orientation, plastic deformation requires greater efforts or higher temperatures. Therefore, the minimum on the temperature dependence of the TLEC in the *T*-direction shifts to higher temperatures. In the case of the axial direction, even higher loads or temperatures are required to activate sliding.

At temperatures of existence of the β-phase (above 920 °C), the TLECs become the same for all studied directions, which correspond to the TLEC of a material with a bcc structure. In the studied samples, a sharp crystallographic texture {0 0 1} ⟨1 1 0⟩ is formed, according to which, upon cooling, the (0001) planes are located in the alloy parallel to the {1 1 0} planes. Fig. 7 shows typical DPFs (0001) and {1 1 $\bar{2}$ 0} for the samples under study, in which the PT texture is formed, which is described in detail in the works [33,34,36,40,52–54].

Analysis of dilatometric curves for a reverse phase transition

The expansion curves are shown in Fig. 4, including the reverse phase transition upon cooling, from which it follows that as a result of the reverse transition of the β-phase to α in samples Nos. 1–3, there is a significant change in dimensions in the *R*-*T*-directions (Table 2). The change in the final dimensions of the samples occurs precisely at the stage of reverse PT in the temperature range 860–600 °C. Taking into account that a sharp crystallographic texture {0 0 1} ⟨1 1 0⟩ was formed in the β-phase, it is possible to calculate the change in dimensions upon precipitation of the α-phase in accordance with the orientational Burgers relations. Since $(0001)_\alpha \,||\, \{1\,1\,0\}_\beta$, the changes in interplanar distance are

$$\varepsilon_c = \frac{d_{0001} - d_{110}}{d_{110}} = \frac{d_{0001}}{d_{110}} - 1 = \frac{c_\alpha}{\sqrt{2}a_\beta} - 1 = 0,0184$$

and $<11\bar{2}0>_\alpha \,||\, \langle 1\,1\,1\rangle_\beta$, then

$$\varepsilon_a = \frac{d_{11\bar{2}0} - d_{111}}{d_{111}} = \frac{d_{11\bar{2}0}}{d_{111}} - 1 = \frac{2a_\alpha}{\sqrt{3}a_\beta} - 1 = 0,0421$$

If we assume that the temperature dependence of the change in the parameters of the crystal structure of the α-phase, presented in [29], remains at the temperature of the onset of reverse phase transitions equal to 860 °C, then $a_\alpha = 324.23$ pm; $c_\alpha = 517.40$ pm. According to the phase diagram and Vegard's law, the β-phase before the reverse phase transition contains 2.5 % Nb and is characterized by the parameter $a\,\beta =$ 359.25 pm. Then $\varepsilon_c = 1.84$ %; and $\varepsilon_a = 4.21$ %. It is clear that, as the material cools in both phases, a redistribution of niobium occurs. In accordance with the phase diagram of Zr-Nb in the β-phase, the concentration of niobium increases faster than in the α-phase. An increase in the niobium content affects the parameters of the crystal structures in the direction of their decrease, since the niobium atom is characterized by a smaller size in comparison with the Zr atom (or ion). A change in temperature has a lesser effect on the periods of crystal cells than the concentration of niobium. Therefore, the real value of the lattice deformation along the *c* and *a* directions will change, but the nature of the changes will remain the same.

So let's take a look at the cooling process. The main regularities are as follows. Three studied samples, which are in different structural states, are characterized by the same behavior upon cooling. In the *L*-direction, the samples experience a minimal increase in size. Along the *R*-direction, the samples decrease in size, and along the tangential direction, a significant increase in the size of the cubic samples is noted (Fig. 4). Note that the change in size occurs in different temperature ranges: 890–780 °C in the *R*- and *L*-directions and 860–550 °C in the *T*-direction.

Let us consider the processes that occur in the considered temperature regions and can lead to an increase or decrease in the size of the samples. On the one hand, this is the formation of the α-phase in the β -matrix associated with an anisotropic increase in the sample size. On the other hand, it is diffusion in the β-phase, which contributes to a decrease in the concentration of zirconium with an increase in the niobium content in accordance with the phase diagram, which leads to a decrease in the lattice period according to Vegard's law and the external dimensions of the sample. The diffusion process is most intensively realized at elevated temperatures under the conditions of an active PT in the temperature range 890–780 °C, which makes it possible to fix the temperature drop in the dependence of the relative change in dimensions for the *R*-direction in Fig. 4-a. However, in the *T*-direction, the PT process is accompanied by an increase in size, which prevails due to an increase in the amount of the α-phase with a decrease in the temperature of the sample as a whole.

It should be noted that the basal axes of the α-phase are located along the *L* and *T* directions, along which the maximum increase in size is noted during the β → α transformation. Prismatic axes are oriented along the radial direction, along which the increase in size does not exceed 2 %, and this is comparable to a decrease in the size of the β-phase. Apparently, in the temperature range 800–860 °C, the effect of the diffusion process in the β-phase dominates, and in the absence of the basal axes in the *R*-direction, it prevails over the process of precipitation of the α-phase, which explains the total decrease in size in the radial direction.

Significant fluctuations in the size of cubic samples in different directions due to the occurrence of phase transformations in the alloy under consideration should lead to the development of significant macrostresses both during heating and during cooling in the case of heating a tube-shaped product.

Conclusions

Based on the results of dilatometric studies of the thermal expansion of the recrystallized Zr-2.5% Nb alloy and the integral texture parameters of Kearns, the averaged coefficients of thermal linear expansion (TLEC) of the α-phase in the *a* and *c* directions were calculated.

The expansion of all investigated samples cut from the wall of pressure tubes upon heating in the α-region of the phase diagram of the Zr-2.5% Nb alloy is determined by the integral texture parameters of Kearns calculated for the radial (*R*), tangential (*T*), and axial (*L*) directions. TLECs in different directions vary from $3{\cdot}10^{-6}$ to $12{\cdot}10^{-6}$ K^{-1}. The nature of the temperature dependence of the TLEC is determined by the structural state and crystallographic texture of the material. The maximum anisotropy of the TLEC is achieved in the samples initially annealed at a temperature of 400 °C for 24 h, and at 500 °C, TLEC (*T*)/ TLEC (*L*) ≈ 3.

During the cooling of the investigated samples at the stage of the reverse phase transformation of the β -phase into α, an increase in their sizes in the tangential direction up to 2.3 % and a decrease in the radial direction up to 1.3 % are noted, if the axes $< 10\bar{1}0 >$ are oriented along *L*-directions in the initial samples. In an alloy characterized by a recrystallization texture with a predominant orientation of the axes $< 11\bar{2}0 >$ along *L*, such large size changes were not found. This behavior of the samples is completely determined by the orientation of the α-phase grains in the-matrix formed upon cooling and the anisotropy of their TLEC.

CRediT authorship contribution statement

M.G. Isaenkova: Conceptualization, Project administration, Methodology, Visualization, Writing – original draft, Writing – review &

editing. **A.V. Tenishev:** Methodology, Validation, Writing – original draft. **O.A. Krymskaya:** Software, Data curation, Writing – original draft. **S.D. Stolbov:** Investigation, Formal analysis, Visualization, Writing – original draft, Writing – review & editing. **V.V. Mikhal'chik:** Investigation. **V.A. Fesenko:** Investigation. **K.E. Klyukova:** Investigation.

Declaration of Competing Interest

The authors declare that they have no known competing financial interests or personal relationships that could have appeared to influence the work reported in this paper.

Acknowledgment

The reported study was funded by RFBR, project number 19-32-90041 and was supported by the MEPhI Academic Excellence Project (agreement with the Ministry of Education and Science of the Russian Federation of August 27, 2013, project no. 02.a03.21.0005).

References

[1] A.V. Nikulina, Structural materials for elements of nuclear-reactor active zones: zirconium alloys in nuclear power engineering // Met, Sci. Heat Treat. 46 (11-12) (2004) 458–462.
[2] Duan Z. et al. Current status of materials development of nuclear fuel cladding tubes for light water reactors // Nuclear Engineering and Design. 2017. Vol. 316. p. 131–150.
[3] D.L. Douglass, The metallurgy of zirconium, Atomic Energy Review, Supplement. International Atomic Energy Agency (1971) 466 p.
[4] W. Li, R.A. Holt, Anisotropic thermal creep of internally pressurized Zr–2,5Nb tubes, Journal of Nuclear Materials 401 (1-3) (2010) 25–37.
[5] V.A. Markelov, Improvement of the composition and structure of zirconium alloys to ensure the operability of fuel elements, fuel assemblies and pressure tubes of water-cooled reactors cores with an increased resource and fuel burnup. Doctor of Science thesis, Moscow (2010) 278 p.
[6] M.G. Isaenkova, Y.A. Perlovich, V.A. Fesenko, S.S. Tkhu, M.M. Peregud, Change in orientation of α-zirconium grains during thermal creep tests, Tsvetnye Metally 12 (2014) 56–61.
[7] A.R. Causey, In-reactor creep of Zircaloy-2, Zircaloy-4 and Zr–1.15wt%Cr–0.1wt% Fe at 568 K derived from their stress-relaxation behavior, Journal of Nuclear Materials 54 (1974) 64–72.
[8] R.A. Holt, In-reactor deformation of cold-worked Zr–2.5Nb pressure tubes, Journal of Nuclear Materials, No. 372 (2-3) (2008) 182–214.
[9] R. Adamson, F. Garzarolli, C. Patterson, In-reactor creep of zirconium alloys, Advanced Nuclear Technology International, Sweden, 2009, p. 144.
[10] SCDAP/RELAP5/MOD3.3 Code Manual, Volume 4: MATPRO – A library of materials properties for light-water-reactor accident analysis. Prepared by L.J. Siefken, E.W. Coryell, E.A. Harvego, J.K. Hohorst. Idaho Falls, Idaho, 2001. – NUREG/CR-6150, Vol. 4, Rev. 2. 713 p.
[11] Material Property Correlations: Comparisons between FRAPCON-4.0, FRAPTRAN-2.0, and MATPRO, September 2015 / WG Luscher KJ Geelhood IE Porter // Pacific Northwest National Laboratory, Richland, Washington 99352. 154 p.
[12] L.R. Bunnell, J.L. Bates, G.B. Mellinger, Some high-temperature properties of zircaloy-oxygen alloys, Journal of Nuclear Materials 116 (2-3) (1983) 219–232.
[13] Y.-H. Koo, J.-H. Yang, J.-Y. Park, K.-S. Kim, H.-G. Kim, D.-J. Kim, Y.-I. Jung, K.-W. Song, KAERI's Development of LWR accident-tolerant fuel, Journal of Nuclear Technology 186 (2) (2014) 295–304.
[14] Kim H.G., Kim I.H., Jung Y.I., Park D.J., Yang J.H., Koo Y.H. Development of surface modified Zr cladding by coating technology for ATF. Conference Top Fuel 2016, Boise, ID, September 11-15, 2016, p. 1157-1163.
[15] H.-G. Kim, J.-H. Yang, W.-J. Kim, Y.-H. Koo, Development status of accident-tolerant fuel for light water reactors in Korea, Nuclear Engineering and Technology 48 (1) (2016) 1–15.
[16] I.A. Petelguzov, Influence of aluminum and chromium covering on oxidation zirconium and some his alloys, VANT. 2 (2012) 114–119.
[17] I.E. Kopanetz, G.D. Tolstolutskaya, A.V. Nikitin, V.A. Bilous, A.S. Kuprin, V. D. Ovcharenko, R.L. Vasilenko, The effect of Cr, Cr-N and Cr-Ox coatings on deuterium retention and penetration in zirconium alloy Zr-1Nb, Problems of Atomic Science And Technology vol. No. 5(99) (2015) 81–86.
[18] Kuprin A.S., Belous V.A., Voyevodin V.N., Bryk V.V., Vasilenko R.L., Ovcharenko V.D., Reshetnyak E.N., Tolmachova G.N., V'yugov P.N. Vacuum-arc chromium-based coatings for protection of zirconium alloys from the high-temperature oxidation in air. Journal of Nuclear Materials, 2015. vol. 465. p. 400-406.
[19] A.S. Kuprin, V.A. Belous, V.V. Bryk, R.L. Vasilenko, V.N. Voyevodin, V. D. Ovcharenko, G.N. Tolmachova, I.V. Kolodiy, V.M. Lunyov, I.O. Klimenko, Vacuum-arc chromium coatings for Zr-1Nb alloy protection against high-temperature oxidation in air, Problems of Atomic Science and Technology 96 (2) (2015) 111–118.
[20] Kuprin A.S., Belous V.A., Voyevodin V.N., Bryk V.V., Vasilenko R.L., Ovcharenko V.D., Tolmachova G.N., V'ygov P.N. High-temperature air oxidation of E110 and Zr-1Nb alloys claddings with coatings. Problems of Atomic Science and Technology, 2014. vol. 89 (No. 1). p. 126-132.
[21] Belous V.A., Výgov P.N., Kuprin A.S., Leonov S.A., Nosov G.I., Ovcharenko V.D., Ozhigov L.S., Rudenko A.G., Savchenko V.T., Tolmacheva G.N., Khoroshikh V.M.. Mechanical characteristics of Zr1Nb alloy tube after deposition of ion-plasma coatings. Problems of Atomic Science and Technology, 2013. vol. 84 (No. 2). p. 140-143.
[22] E.V. Berlin, V.Yu. Grigoriev, A.V. Ivanov, M.G. Isaenkova, K.E. Klyukova, S. D. Stolbov, Structure of the protective chromium coating obtained by a thermal evaporation method in a magnetron discharge on the cladding tube from E110 alloy, Tsvetnye Metally (2019) 33–40, https://doi.org/10.17580/tsm10.17580/tsm.2019.04.04.
[23] Isaenkova M.G., Perlovich Y.A., Stolbov S.D., Klyukova K.E., Fesenko V.A., and Berlin E.V. Influence of technology of obtaining chromium coating on cladding tubes from Zr – 1% Nb – (O, Fe) alloy on change of its structure during air oxidation at temperatures 400–1150°C Tsvetnye Metally, 2020. vol. 2020, No. 2. p. 66-75.
[24] R.L. Mehan, F.W. Wiesinger, Mechanical properties of Zircaloy-2, KAPL-2110, General Electric Company, Knolls Atomic Power Laboratory, Schenectady, New York 1961 (1961) 11–12.
[25] D.B. Scott, Physical and mechanical properties of Zircaloy 2 and 4, WCAP-3269-41, 9 / Westinghouse Electric Corporation, Pittsburgh, Pennsylvania, Atomic Power Division, 1965, p. 71.
[26] Kearns J.J. 1965 Thermal expansion and preferred orientation in Zircaloy (Bettice Atomic Power Laboratory Report WAPD-TM-472). WAPD-TM-472, TID-4500, Nov. 1965. Bettis Atomic Power Lab., Pittsburgh P.A. 37 p.
[27] P.F. Prasolov, V.E. Shestak, P.A. Platonov, O.K. Chugnov, V.F. Viktorov, Anisotropy of the elastic modulus and thermal-expansion coefficient of textured zirconium alloys N-1 and N-2.5. Soviet, Atomic Energy 68 (2) (1990) 113–118.
[28] M.G. Isaenkova, A.V. Tenishev, Yu.A. Perlovich, S.D. Stolbov, V.V. Mikhalchik, P. V. Fedotov, V.V. Novikov, V.I. Kuznetsov, Thermal expansion of cladding tubes and rods made of Zr-1% Nb alloy in the temperature range of 293–873 K (20–600 °C) according to the results of X-ray and dilatometric measurements, Physics and chemistry of materials treatment 3 (2020) 53–65.
[29] Isaenkova, M. G. Tenishev, A. V. Perlovich, Yu. A. Stolbov, S. D. Mikhalchik, V. V. Fedotov, P. V. Novikov, V. V. Kuznetsov, V. I. Regularities of Thermal Expansion of Cladding Tubes and Rods Made of E110opt Alloy within the Temperature Range of 273–1473 K (20–1200°C). Inorganic Materials: Applied Research, 2021, Vol. 12, No. 3, p. 820–830.
[30] M.G. Isaenkova, Yu.A. Perlovich, V.A. Fesenko, O.A. Krymskaya, N.A. Krapivka, Soe San Tkhu, Regularities of recrystallization of rolled single crystals and polycrystals of zirconium and alloy Zr-1% Nb, Physics of Metals and Metallography 115 (8) (2014) 756–764.
[31] A.K. Shikov, O.V. Bocharov, V.M. Arzhakova, V.N. Bezumov, Yu.A. Perlovich, M. G. Isaenkova, Use of hafnium in control elements of nuclear reactors and power units, Metal Science and Heat Treatment 45 (7–8) (July 2003) 300–303.
[32] M.G. Isaenkova, Yu.A. Perlovich, S.S. Thu, O.A. Krymskaya, V.A. Fesenko, Development of crystallographic texture in the time of rolling of Zr monocrystals and their recrystallization, Tsvetnye Metally 12 (2014) 73–78.
[33] M.G. Isaenkova, Perlovich Yu A Regularities of the development of crystallographic texture and substructural heterogeneity in zirconium alloys during deformation and heat treatment, Moscow, NRNU MEPhI. (2014) 528 p (in Russian).
[34] U.F. Kocks, C.N. Tome, H.R. Wenk, Texture and anisotropy, Cambridge University Press, 1998, p. 675 p..
[35] Fong R.W.L., Fazeli F., Smith T. Thermal expansion anisotropy of Zr-2.5Nb pressure tube material on heating to 1100°C, 35th Annual Conference of the Canadian Nuclear Society, Canada, Gaëtan Thomas, Jacques Plourde, Ben Rouben, Kathleen Duguay, Curran Associates, Incorporated, 2015. p. 1-12.
[36] R.W.L. Fong, R. Miller, H.J. Saari, S.C. Vogel, Crystallographic texture and volume fraction of α and β phases in Zr-2.5Nb pressure tube material during heating and cooling, Metallurgical and Materials Transactions A 43 (3) (2012) 806–821.
[37] B.A. Cheadle, C.E. Ells, The effect of heat treatment on the texture of fabricated Zr-rich alloys, – Electroch. Techn. 4 (7–8) (1966) 329–336.
[38] J. Romero, M. Preuss, J. Quinta da Fonseca, Texture memory and variant selection during phase transformation of a zirconium alloy, Acta Materialia 57 (18) (2009) 5501–5511.
[39] Chi-Toan Nguyen, Javier Romero, Antoine Ambard, Michael Preuss, João Quinta da Fonseca, The effect of cold work on the transformation kinetics and texture of a zirconium alloy during fast thermal cycling, Materials Science and Engineering A 746 (2019) 424–433.
[40] M. Isaenkova, Yu. Perlovich, Features of the phase transformations in sheets, tubes and welding seams of the alloy Zr-2,5%Nb, Textures and Microstructures 30 (1-2) (1997) 55–70.
[41] T. Jailin, N. Tardif, J. Desquines, M. Coret, M.-C. Baietto, V. Georgenthum, Experimental study and modelling of the phase transformation of Zircaloy-4 alloy under high thermal transients, Materials Characterization 162 (2020) 110199, https://doi.org/10.1016/j.matchar.2020.110199.
[42] L. Chai, J. Xia, Y. Zhi, K. Chen, T. Wang, B. Song, N. Guo, Strengthening or weakening texture intensity of Zr alloy by modifying cooling rates from α + β region, Materials Chemistry and Physics 213 (2018) 414–421.
[43] M Isaenkova, Yu Perlovich, V Fesenko, Modern methods of experimental construction of texture complete direct pole figures by using X-ray data. IOP Conf. Series, Materials Science and Engineering 130 (2016) 012055, https://doi.org/10.1088/1757-899X/130/1/012055.

[44] J.F. Nye, Physical properties of crystals: Their representation by tensors and matrices, Clarendon Press, Oxford, 1964, p. 322.
[45] Shishov V.N., Nikulina A.V., Markelov V.A., Peregud M.M., Kozlov A.V., Averin A. V., Kolbenkov S.F., Novoselov A.E., Influence of Neutron Irradiation on Dislocation Structure and Phase Composition in Zr-Base Alloys. 11th International Symposium on Zr in the Nuclear Industry, Garmisch-Partenkirchen, Germany, E. R. Bradley and G. P. Sabol, West Conshohocken, PA, Eds. ASTM International 1996 (1995) 603–622.
[46] Nikulina A.V., Shishov V.N., Peregud M.M., Tselishchev A.V., Shamardin V.K., Kobylyansky G.P. Irradiation Induced Growth and Microstructure Evolution of Zr-1.2Sn-1Nb-0.4Fe Under Neutron Irradiation to High Doses. 18th Symposium on Effects of Radiation on Materials, R.K Nanstad, M.L.Hamilton, F.A.Garner, West Conshohocken, PA, Eds. ASTM International, 1999. p. 1045-1061.
[47] Shishov V. N., Peregud M. M., Nikulina A. V., Shebaldov P. V., Tselishchev A. V., Novoselov A. E., Kobylyansky G. P., Ostrovsky Z. E., Shamardin V. K., Influence of Zirconium Alloy Chemical Composition on Microstructure Formation and Irradiation Growth, 13th International Symposium on Zirconium in the Nuclear Industry, Annecy, France, G. D. Moan and P. Rudling, West Conshohocken, PA, Eds. ASTM International 2002 (2001) 758–779.
[48] H.J. Bunge Yu. Perlovich M. Isaenkova V. Fesenko N.J. Park L. Wcislak M. Zuev Inhomogeneity of phase transformations β→ α and β→α in the quenched cold-rolled alloy Zr-20%Nb J. de Physique IV, Colloque C6, supplement au J.de Physique III 6 1 1996 pp. C1–149 – C1–156.
[49] M Griffiths, JF Mecke, JE Winegar, in: Zirconium in the Nuclear Industry: Eleventh International Symposium, ASTM International, 100 Barr Harbor Drive, PO Box C700, West Conshohocken, PA 19428-2959, 1996, pp. 580–580-23, https://doi.org/10.1520/STP16191S.
[50] Chernyaeva T.P., Gritsina V.M., Mikhailov E.A., Vasilenko R.L., Slabospitskaya E.A. Structural features of quenched Zr-Nb – VANT: Physics of radiation damage and radiation materials science, 2011. №2. p. 95-107.
[51] F. Gerspach, N. Bozzolo, F. Wagner, About texture stability during primary recrystallization of cold-rolled low alloyed zirconium, Scr. Mater. Acta Materialia Inc. 60 (4) (2009) 203–206.
[52] Isaenkova M.G., Perlovich Yu.A., Shmelyova T.K., Nikulina A.V., Zav'yalov A.R. Change in the texture of tubes made of Zr – 2.5% Nb alloy upon recrystallization. – Atomic Energy, 1989. vol. 67 №5. p. 327-331.
[53] Isaenkova M., Perlovich Yu. Regularities of recrystallization in sheets and tubes of Zr-alloys. – In: Microstructural and Crystallographic Aspects of Recrystallization. Ed.N.Hansen et al. Riso National Lab., Roskilde, Denmark, 1995, p. 371-376.
[54] Isaenkova M.G., Perlovich Y.A., Fesenko V.A., Solov'yov V.N., Sergacheva M.I., Krymskaya, O.A., Tkhu S.S., Novikov V.V., Kabanov A.A. Influence of technological parameters of manufacturing of cladding tubes on their crystallographic texture. Tsvetnye Metally, 2014. №12, p. 62-67.